Convective Mass Transfer From Submerged Superhydrophobic Surfaces

Christina A. Barth[1], Mohamed A. Samaha[2], Hooman Vahedi Tafreshi[1] and Mohamed Gad-el-Hak[1]
[1]Department of Mechanical & Nuclear Engineering, Virginia Commonwealth University, Richmond, VA 23284
[2]Department of Mechanical & Aerospace Engineering, Princeton University, Princeton, NJ 08544

Received date 5/4/2013; Accepted date 6/6/2013

Abstract
Longevity of entrapped air is an outstanding problem for using superhydrophobic coatings in submersible applications. Under pressure and flowing water, the air micropockets eventually dissolve into the ambient water or burst and diminish. Herein, we analyze from first principles a simple mass transfer problem. We introduce an effective slip to a Blasius boundary layer, and solve the hydrodynamic equations. A slowly evolving, non-similar solution is found. We then introduce the hydrodynamic solution to the two-dimensional problem of alternating solid–water and air–water interfaces to determine the convective mass transfer of air's dissolution into water. This situation simulates spanwise microridges, which is one of the geometries used for producing superhydrophobic surfaces. The mass-transfer problem has no similarity solution but is solvable using approximate integral methods. A mass-transfer solution is achieved as a function of the surface geometry (or gas area fraction), Reynolds number, and Schmidt number. The analytical results are compared to numerical simulations of the laminar Navier–Stokes equations. Longevity, or time-dependent hydrophobicity, can be estimated from the resulting mass-transfer correlation.

1. INTRODUCTION

Superhydrophobic coatings possess a strong water-repellent characteristic, which enhances the mobility of water droplets over such surfaces [1]. The coating traps air within its micropores, such that a submerged, moving body experiences shear-free and no-slip regions over, respectively, the air pockets and the solid surface. This, in turn, may lead to significant skinfriction reduction [2, 3]. Additional applications of hydrophobic surfaces include enhancing evaporation [4–6], hindering frost [7–10], and resisting corrosion [11, 12].

A popular method of manufacturing a superhydrophobic surface is microfabrication in which microridges or posts are placed on a surface in a regular configuration [13–15]. The orientation with respect to the flow, spacing, and aspect ratio of the microposts or microridges can be adjusted to optimize the drag reduction [16] and the stability of the air–water interface [17] against transition from dewetted Cassie [18] to wetted Wenzel [19] state.

The coating maintains its superhydrophobicity as long as the air remains entrapped. Even when the air–water interface on a submerged superhydrophobic surface is mechanically stable, the surface is likely to lose its entrapped air over time. This effect is believed to be due to the dissolution of air into water, and is expected to accelerate when the hydrostatic pressure is increased, as the solubility of air into water increases with pressure [20, 21], and when the flow speed increases, which enhances convective mass transfer [22]. Several approaches have recently been developed to measure the longevity of superhydrophobic surfaces [20, 23–25]. Analytical approaches are lacking, however, due to the complexity of the problem.

In this work, we present a first-principles model to predict the rate of mass transfer of air from superhydrophobic surfaces with spanwise ridges. We assume a two-dimensional, laminar boundary flow over such a surface and solve the decoupled hydrodynamic and mass transfer problems. A single-phase flow is assumed, and the air pockets supply only a linearized boundary condition. While more

detailed models exist, their solutions are more complex and limited than the method presented herein [16, 26–28].

The theoretical approach is described in the next section. Section 3 discusses the numerical simulations used. Comparison between the theoretical and numerical results is demonstrated in Section 4. This is followed by Section 5 in which the results are presented and a mass-transfer correlation is developed. Conclusions are given in Section 6.

2. THEORETICAL APPROACH

We consider laminar boundary layer flow over a superhydrophobic surface comprised of spanwise microridges, as shown in Figure 1. The solution is obtained for different Reynolds numbers (based on plate length), Schmidt numbers (ratio of water kinematic viscosity to mass diffusivity of air into water), and gas fractions (ratio of shear-free surface area to total surface area). The hydrodynamic boundary layer thickness $\delta(x)$ continuously evolves in the flow direction. After a starting length of 1 cm, the plate is considered as alternating sections of no-slip solid–water interface with zero concentration of air (C_∞) and free-shear air–water interface with 100% saturation of air (C_s). At each change in position x_1, x_2, $\cdots$, there is a newly growing mass-transfer boundary layer thickness, $\delta_c(x)$, due to the abrupt change in the concentration boundary condition. The pitch of the superhydrophobic surface is fixed at 200 μm. Gas fraction increases are achieved by reducing the width of each ridge. The solution is obtained for a total of ten consequent sections (five peaks and five troughs). The hydrodynamic boundary layer solution is obtained using a modified Blasius model with an effective slip, while the decoupled mass transfer problem is solved using the approximate integral method.

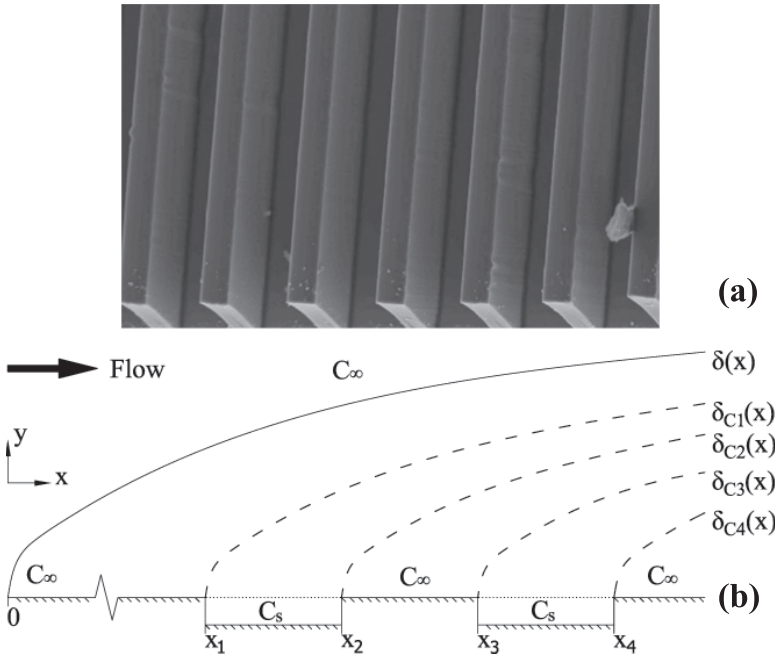

Figure 1: (a) SEM image of spanwise ridges to effect superhydrophobicity, from Maynes et al. [16] (b) Schematic of both hydrodynamic and mass-transfer boundary layers evolving over microridges.

Strictly speaking, the concentration boundary condition at the solid–water interface downstream of the starting length should be $[\partial C/\partial y]_{y=0} = 0$. The boundary condition at the air– water interface is correct as stated above, $[C]_{y=0} = C_s$. However, the use of mixed Dirichlet and Neumann boundary conditions would preclude the employment of the superposition principle to be described in Section 2.1. The present model, though difficult to realize in practice, provides a first-principles analytical result, which is indeed rare. In the analogous heat transfer problem, alternating hot and ambient temperatures are

used. This situation requires heated and cooled portions of the plate, which is different from heated and unheated portions.

2.1 Mass Transfer Solution Using Integral Method

The mass-transfer integral is derived via manipulation of the species conservation equation. The integral normal to the wall reduces to the following numerically solvable integrodifferential equation [29]:

$$\frac{d}{dx}\int_0^{\delta_c(x)} u(y)\left[\vartheta_\infty - \vartheta(y)\right] dy = D\left(\frac{\partial C}{\partial y}\right)_{wall} \tag{1}$$

where D is the mass diffusivity of air into water, $\delta_c(x)$ is the concentration boundary layer thickness, and $\vartheta(y)$ is the approximate concentration profile, which for a typical laminar boundary layer takes the form [30]:

$$\vartheta(y) = C(y) - C_{wall} \;\&\; \vartheta_\infty = C_\infty - C_{wall} : \vartheta(y) \approx \vartheta_\infty\left(\frac{3}{2}\frac{y}{\delta_c(x)} - \frac{1}{2}\frac{y^3}{\delta_c(x)^3}\right) \tag{2}$$

where C_{wall} is the concentration at the wall, and $C(y)$ is the concentration distribution below $\delta_c(x)$.

In our solution, the velocity profile, $u(y)$, and the hydrodynamic boundary layer thickness, $\delta(x)$, are obtained from the solution of the hydrodynamic problem, as discussed in detail in Section 2.2. Note that in the present *approximate* integral method, other approximate velocity profiles could also be used. For example, those resulting from a third-order polynomial fit.

The mass transfer coefficient h_m and its dimensionless equivalent Sherwood number $Sh_x \equiv h_m\, x/D$ are found from the relationship between the molar flux transfer equation, the convective molar flux equation, and Fick's law [31]. Thus, $h_m = \frac{3}{2}(D/\delta_c(x))$ and $Sh_x = \frac{3}{2}(x/\delta_c(x))$.

It is observed that the only impact of the no-slip assumption on the integral method is in the input of $u(y)$, which we create as an effective slip velocity profile. The slip Blasius solution can output u in the region $y < \delta(x)$. One can omit the step of finding $\delta(x)$ from the hydrodynamic equations and proceed directly to the mass transfer solution of the integral method.

The integral method can be altered to find the value of the local mass flux m'' over a plate with arbitrary wall concentrations. Bejan [29] describes the process for heat transfer, noting that the derivations for heat flux and mass flux are analogous. This m'' is found by observing that due to the newly growing $\delta_c(x)$ at each abrupt change in concentration, there are also newly growing values of $h_m(x)$. Since the decoupled concentration equation is linear, the local m'' is found by using superposition along the plate

$$m'' = h_m(x)\Delta C \tag{3}$$

where $h_m(x)$ is the sum of all the newly growing $h_m(x)$ at and prior to that local section or change in wall concentration, and ΔC is the change in concentration between the microridges.

To find the average mass flux $\overline{m''}$, the total average mass transfer coefficient $\overline{h}_m$ must first be computed. The total $\overline{h}_m$ is the summation of all the local $\overline{h}_m$. Thus

$$\overline{h}_{m_{Total}}\mathcal{L} = \overline{h}_{m_1}(x_2 - x_1) + \overline{h}_{m_2}(x_3 - x_2) + \overline{h}_{m_3}(x_4 - x_3) + \overline{h}_{m_4}(x_5 - x_4) + \cdots \tag{4}$$

where $\mathcal{L}$ is the length of the entire superhydrophobic region, and the local $\overline{h}_m$ is computed as follows

$$\begin{aligned} \overline{h}_{m_1} &= \frac{\int_{x_1}^{x_2} h_{m_1}(x)dx}{x_2 - x_1};\ \overline{h}_{m_2} = \frac{\int_{x_2}^{x_3} h_{m_1}(x)dx}{x_3 - x_2} - \frac{\int_{x_2}^{x_3} h_{m_2}(x)dx}{x_3 - x_2};\\ \overline{h}_{m_3} &= \frac{\int_{x_3}^{x_4} h_{m_1}(x)dx}{x_4 - x_3} - \frac{\int_{x_3}^{x_4} h_{m_2}(x)dx}{x_4 - x_3} + \frac{\int_{x_3}^{x_4} h_{m_3}(x)dx}{x_4 - x_3};\cdots \end{aligned} \tag{5}$$

The summation in Equation (4) is accurate for any gas fraction ϕ_g, and does not require equidistant segments of the microridges. Equations (4) and (5) could be combined and generalized to yield

$$\overline{h}_{m_{Total}} = \mathcal{L}^{-1} \sum_{j=1}^{n} \sum_{i=1}^{j} (-1)^{i+1} \int_{x_j}^{x_{j+1}} h_i(x) dx \tag{6}$$

where n is the total number of peaks and troughs (ten in the present formulation).

2.2 Blasius Boundary Layer for Slip Flow

The classical Blasius boundary layer uses the no-slip boundary assumption at the wall. Following [32, 33], this assumption is relaxed due to the slip flow effect of superhydrophobic surfaces. We use the effective slip boundary condition of Navier [34]:

$$u_{wall} = S \left(\frac{\partial u}{\partial y} \right)_{wall} \tag{7}$$

where u_{wall} is the streamwise slip velocity at the wall, $(\partial u/\partial y)_{wall}$ is the magnitude of the wall strain rate, and S is the slip length. The effective S could be estimated via experimental observations [35] or numerical simulations [14, 36]. Herein we estimate the slip length for each gas fraction using numerical simulations of the two-dimensional, laminar Navier–Stokes equations, as explained in Section 3.

According to the classical Blasius solution [37], the momentum and continuity equations can be reduced to the third-order ordinary differential equation

$$f(\eta) f''(\eta) + 2f'''(\eta) = 0 \tag{8}$$

where $f(\eta)$ is the dimensionless stream function, $\eta \equiv y/\delta(x)$ is the similarity coordinate, and $'$ denotes derivative w.r.t. η. The streamwise velocity component can be expressed in terms of the freestream velocity as $u = U_\infty f'(\eta)$. The boundary conditions, modified to admit slip, are

$$\text{At } y = 0 : u = u_{wall} = S \left(\frac{\partial u}{\partial y} \right)_{wall}, \; v = 0; \text{at } y = \infty : u = U_\infty \tag{9}$$

where v is the normal velocity component. The boundary conditions can be rewritten in terms of f and η as

$$\text{At } \eta = 0 : f(\eta) = 0, \; f'(\eta) = \frac{S}{x} \times f''(0) \sqrt{Re_x}; \text{ at } \eta = \infty : f'(\eta) = 1 \tag{10}$$

where $Re_x = U_\infty x/\nu$ is the Reynolds number, and ν is the kinematic viscosity of water.

Martin and Boyd [32] point out that self-similarity is lost because of the slip boundary

condition (10), which depends on x, and that the velocity will be a function of both η and the dimensionless slip length given by

$$S^* = \frac{S}{x} \sqrt{Re_x} \tag{11}$$

At the wall, $\partial u/\partial x$ is no longer zero, and therefore, $\partial v/\partial y$ is also not zero. Mathematically, the inhomogenous wall boundary condition breaks down the similarity. The normal velocity is modified to incorporate the derivative of the stream function with respect to S^*. When all other derivatives in x are rewritten to include S^*, the ordinary differential equation (8) becomes a partial differential equation with an additional term that is proportional to the slip length

$$f\frac{\partial^2 f}{\partial \eta^2} + 2\frac{\partial f^3}{\partial \eta^3} + S^*\frac{\partial}{\partial \eta}\left[\frac{\partial f}{\partial \eta}\frac{\partial f}{\partial S^*}\right] = 0 \tag{12}$$

The slip velocity and the change of f with slip length are, however, very small and therefore the obtained solution over the relatively small extent of the microridges is not too far from that using a slowly evolving Blasius profile with an indicated slip. Nevertheless, we numerically integrated, using Mathematica, the exact equation derived by Martin and Boyd [32] and the boundary conditions given therein. The 1-mm section of the plate containing microridges was divided into fifty, 20-μm subsections, and the integral in Equation (1) was carried out.

3. NUMERICAL SIMULATIONS

The present study focuses on the steady, two-dimensional, incompressible, laminar flow of water over a superhydrophobic surface comprised of spanwise ridges, with consideration for air mass transfer between the ridges. The problem is simplified by considering only a singlephase flow of water. In other words, the air between the microridges only effects a shear-free boundary condition at each air–water interface. Meniscus effects are also neglected. Those effects can be included, but not without added complexity to the problem [26]. To supply the effective slip length as well as to validate the integral method results, numerical simulations of the continuity, momentum, and mass transfer equations are carried out using FLUENT. A user defined function (UDF) for the mass diffusivity of air into water (e.g., $D = 2.5 \times 10^{-9}$ m^2 /s at STP) is built using c++ programming language and loaded to FLUENT.

$$\frac{\partial u_i}{\partial x_i} = 0 \tag{13}$$

$$\rho u_j \frac{\partial u_i}{\partial x_j} = -\frac{\partial p}{\partial x_i} + \mu\frac{\partial}{\partial x_j}\left(\frac{\partial u_i}{\partial x_j}\right) \tag{14}$$

$$\rho u_j \frac{\partial C}{\partial x_j} = D\frac{\partial}{\partial x_j}\left(\frac{\partial C}{\partial x_j}\right) \tag{15}$$

where u_i is the velocity field, x_i are the Cartesian coordinates, ρ is the fluid density, p is the pressure, μ is the water viscosity, and C is the air concentration in water. We only simulated the flow over the microridges, with a velocity inlet boundary condition, at a location of 0.99 cm from the leading edge, obtained from the classical Blasius solution. The outlet boundary condition at the end of the plate is zero pressure. Symmetry boundary condition is assigned outside the boundary layer. A no-slip condition is imposed at the solid–water interface, while a shear-free boundary condition is imposed at the air-water interface

$$\frac{\partial u_i}{\partial y}\Big|_{y=0} \approx 0 \tag{16}$$

The concentration boundary conditions are distributed as shown in Figure 1. The saturation boundary condition of air in water C_s is calculated using Henry's law at atmospheric pressure and 20°C [22]. The numerical domain was meshed using 250,000 square cells (2.5 × 2.5 μm). Mesh independence was observed at this resolution.

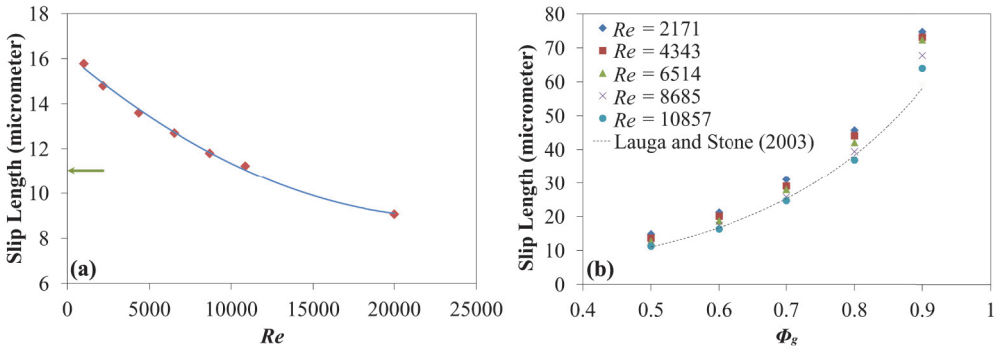

Figure 2: (a) Slip length versus Reynolds number at 50% gas fraction. Present numerical simulations (solid diamonds), and equation of Lauga and Stone [36] at low *Re* (green arrow).(b) Slip length versus gas fraction.

4. VALIDATION

4.1 Slip Length

Figure 2a shows the influence of Reynolds number on the slip length using the numerical simulations at 50% gas fraction. It is clear that the slip length decreases with Reynolds number increase. The slip length is calculated using the numerically estimated area-weighted average slip velocity and velocity gradient at the superhydrophobic wall, which both increase with Reynolds number. It appears that the increase rate of the velocity gradient is larger than that of the slip velocity, which leads to a reduction in the slip length with *Re* increase. For reference, the figure also shows the slip length (the green arrow) at the same gas fraction computed from the equation of Lauga and Stone [36]. Their result was developed for a creeping, pressure-driven flow through a pipe with spanwise microridges. Figure 2b shows the effect of ϕ_g on the slip length at different Reynolds numbers. It is clear that the slip length increases exponentially with gas fraction for superhydrophobic surfaces comprised of microridges, which, despite the different flow regime and geometry, agrees well with the equation of Lauga and Stone [36].

4.2 Sherwood Number

For further validation, we compared the Sherwood number calculated using the integral method with that obtained from the Navier–Stokes simulations. In both cases, the Sherwood number is averaged over the 1 mm extent of the superhydrophobic region. The results are plotted versus Reynolds number at 50% gas fraction, as shown in Figure 3. It is clear that as the Reynolds number increases, the Sherwood number increases indicating higher rate of air dissolution into water. It can also be seen that the results of the approximate integral method are in close agreement with the more-exact numerical simulations. Both indicate a power-law dependence, with an exponent of 0.53 for the former method and 0.49 for the latter. Within the limitations of the present model, the integral method provides fairly accurate results, and longevity can therefore be calculated from first principles.

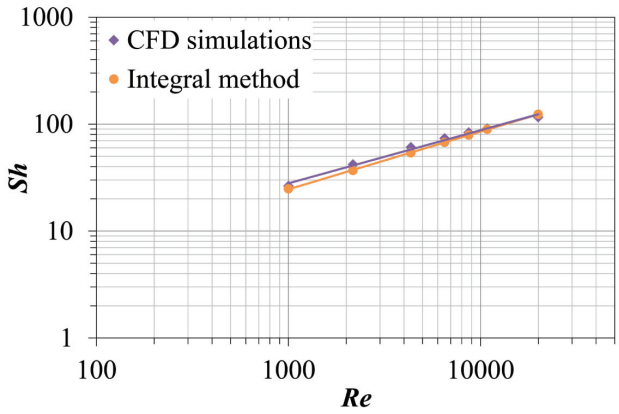

Figure 3: Sherwood number versus Reynolds number. Comparison between the integral method and the numerical simulations. Schmidt number = 400; Gas fraction = 50%.

5. RESULTS AND DISCUSSION

5.1 Effect of Reynolds Number and Schmidt number

Using the approximate integral method , we calculate the dimensionless air mass-transfer convection coefficient (Sherwood number) for spanwise microridges subjected to laminar flow with different Reynolds numbers and Schmidt numbers. Reynolds number is changed in the range of 1,000–10,857, by changing the flow speed and maintaining a fixed plate length. Schmidt number is changed in the range of 200–1,000, which corresponds to changing the water temperature in the range of 35–5°C. The surfaces have different gas fractions ranging from 50–90%. We considered this range of gas fraction because below 50%, the slip length is too small to sustain superhydrophobicity, and above 90%, the longevity diminishes appreciably.

Figure 4a shows Sherwood number versus gas fraction at five different Reynolds numbers. It can be seen that as gas fraction increases, the convection coefficient increases. We reason that the increase in gas fraction increases the area of air–water interface, which leads to augmentation of the mass transfer. The figure also shows that increasing the Reynolds number results in higher convection coefficient. Increasing flow velocity enhances the dissolution of entrapped air into water, as has been shown experimentally by Samaha et al. [22].

We also estimate the convection coefficient at five different Schmidt numbers, as shown in Figure 4b. As the Schmidt number increases, Sherwood number increases, agreeing with the canonical case of no-slip Blasius flow for either heat or mass transfer.

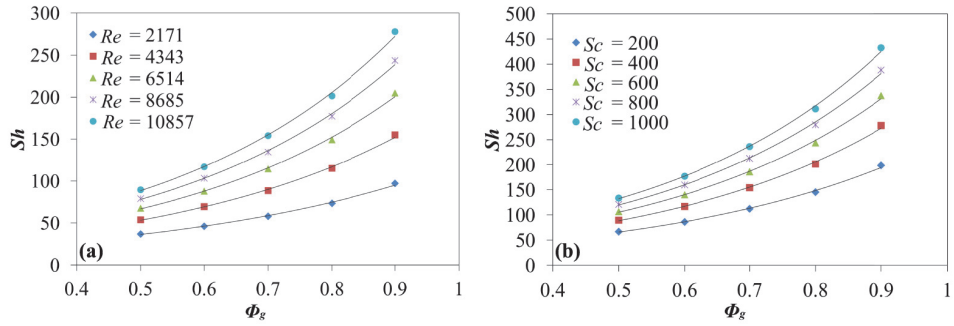

Figure 4: Dimensionless mass transfer convection coefficient versus gas fraction. (a) At different Reynolds numbers with Sc = 400. (b) At different Schmidt number with Re = 10,857.

5.2 Longevity

Longevity of superhydrophobic surfaces depends on how long the surface can entrap air. The present results indicate how the flow affects the dissolution of air into water via convective mass transfer. Figure 5 shows the rate of mass flux corresponding to the results presented in Figure 4. Again, increasing the gas fraction or Reynolds number results in accelerating the rate at which air dissolves into water, or in reduced longevity. On the other hand, increasing the Schmidt number reduces the air mass transfer owing to the reduction in the mass diffusivity D of air into water.

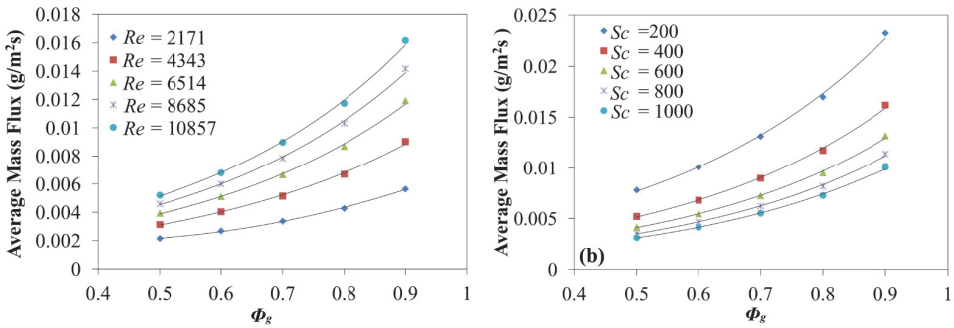

Figure 5: Average air mass flux versus gas fraction. (a) At different Reynolds numbers with Sc = 400. (b) At different Schmidt number with Re = 10,857.

5.3 Mass-Transfer Correlation

It is useful to develop a mass-transfer correlation of the form

$$Sh = f(Re, Sc, \phi_g) \tag{17}$$

The classical correlation for mass-transfer forced convection from a solid flat plate subjected to a laminar, Blasius flow reads

$$Sh_x = 0.332 Re_x^{1/2} Sc^{1/3} \tag{18}$$

As $\phi_g \to 1$, there is near perfect slip, and the hydrodynamic boundary layer is very small compared to the concentration boundary layer. In that case, $u(y) \approx U_\infty$, and Equation (15) could readily be integrated. The solution is

$$Sh_x = \frac{1}{\sqrt{\pi}} Re_x^{1/2} Sc^{1/2} \tag{19}$$

We propose the following correlation for the ranges of Re, Sc, and ϕ_g investigated

$$Sh = K \phi_g Re^{1/2} Sc^{(\frac{1}{3} + \frac{\phi_g}{6})} \tag{20}$$

where Sh is the Sherwood number averaged over the superhydrophobic region. Fitting the data presented in Figure 4, we arrive at $K = 0.145 \pm 0.01$. In the limit of $\phi_g = 0$, there is no mass transfer and $Sh = 0$.* At small ϕ_g, the exponent of Sc reduces to $\approx 1/3$, the same exponent as in the classical equation (18). At $\phi_g = 1$, the exponent of Sc is 1/2, the same as the perfect slip case described by Equation (19). Finally, we also allowed an arbitrary exponent for the first gas fraction appearing in Equation (20). At 1.168 ± 0.08, the resulting exponent is very close to the unity exponent originally hypothesized. In the case of an exponent slightly larger than one, the concomitant constant of proportionality K increases by 3.6%.

6. CONCLUSIONS

In this work, a first-principles model was used to predict the rate of convective mass transfer of air from superhydrophobic surfaces subjected to laminar flow. Blasius-like solution was used to solve the hydrodynamic problem with slip boundary condition. The mass transfer problem was solved using the integral method, and a mass-transfer correlation was developed. The estimated rate of mass transfer reflects how long the surface can keep its hydrophobicity, i.e., longevity. This work could be extended to solve two-dimensional and axi-symmetric turbulent boundary layers without reverting to the computer-intensive direct numerical simulations.

ACKNOWLEDGMENTS

This research is sponsored by the Defense Advanced Research Projects Agency (DARPA), contract numbers W91CRB-10-1-0003 and W911QX-12-1-0001, technical sponsor Captain Christopher Warren, USN. The content of this paper does not necessarily reflect the position or the policy of the United States Government, and no official endorsement should be inferred. We thank Drs. Michael J. Martin and Iain D. Boyd of the University of Michigan for a fruitful discussion.

*Note that if the plate is strictly solid, in contrast to porous, the convection described in Equation (18) can only occur via such processes as evaporation or sublimation.

REFERENCES

[1] Neinhuis, C., Barthlott, W., Characterization and distribution of water-repellent, self-cleaning plant surfaces, *Ann. Bot.*, 1997, 79(6), 667–677.

[2] Rothstein, J. P., Slip on superhydrophobic surfaces, *Annu. Rev. Fluid Mech.*, 2010, 42, 89–109.

[3] Samaha, M. A., Tafreshi, H. V., Gad-el-Hak, M., Superhydrophobic surfaces: From the lotus leaf to the submarine, *C. R. Mec.*, 2012, 340(1), 18–34.

[4] Lee, C. Y., Zhang B. J., Park, J., Kim, K. J., Water droplet evaporation on Cu-based hydrophobic surfaces with nano and micro-structures, *Int. J. Heat Mass Transfer*, 2012, 55(7–8), 2151–2159.

[5] Ojha, M, Chatterjeea, A., Mont, F., Schubert, E. F., Wayner, P. C. Jr., Plawsky, J. L., The role of solid surface structure on dropwise phase change processes, *Int. J. Heat Mass Transfer*, 2010, 53(5), 910–922.

[6] Srikar, R., Gambaryan-Roisman, T., Steffes, C., Stefan, P., Tropea, C., Yarin, A. L., Nanofiber coating of surfaces for intensification of drop or spray impact cooling, *Int. J. Heat Mass Transfer*, 2010, 52(25), 5814–5826.

[7] Kulinich, S. A., Farhadi, S., Nose, K., Du, X. W., Superhydrophobic surfaces: Are they really ice-repellent?, *Langmuir*, 2011, 27(1), 25–29.

[8] Liu, Z., Gou, Y., Wang, J., Cheng, S., Frost formation on a superhydrophobic surface under natural convection conditions, *Int. J. Heat Mass Transfer*, 2008, 51(25), 5975–5982.

[9] Liu, Z., Zhang, X., Wang, H., Meng, S., Cheng, S., Influences of surface hydrophilicity on frost formation on a vertical cold plate under natural convection conditions, *Experimental Thermal and Fluid Science*, 2007, 31(7), 789–794.

[10] Rahman, M. A., Jacobi, A. M., Drainage of frost melt water from vertical brass surfaces with parallel microgrooves, *Int. J. Heat Mass Transfer*, 2012, 55(5), 1596–1605.

[11] Zhang, F., Zhao, L., Chen, H., Xu, S., Evans, D. G., Duan, X., Corrosion resistance of superhydrophobic layered double hydroxide films on aluminum, *Angrew. Chem. Int. Ed.*, 2008, 47(13), 2466–2469.

[12] Grignard, B., Vaillant, A., de Coninck, J., Piens, M., Jonas, A. M., Detrembleur, C., Jerome, C., Electrospinning of a functional perfluorinated block copolymer as a powerful route for imparting superhydrophobicity and corrosion resistance to aluminum substrates, *Langmuir*, 2011, 27(1), 335–342.

[13] Ou, J., Perot, J. B., Rothstein, J. P., Laminar drag reduction in microchannels using ultrahydrophobic surfaces, *Phys. Fluids*, 2004, 16, 4635.

[14] Ybert, C., Barentin, C., Cecile, C. -B., Jospeh, P., Bocquet, L., Achieving large slip with superhydrophobic surfaces: scaling laws for generic geometries, *Phys. Fluids Rev. Lett.*, 2007, 19, 123601.

[15] Lee, C., Choi, C-H., Kim, C-J., Structured surfaces for giant liquid slip, *Phys. Rev. Lett.*, 2008, 101(6), 064501.

[16] Maynes, D., Jeffs, K., Woolford, B., Webb, B. W., Laminar flow in a microchannel with hydrophobic surface patterned microribs oriented parallel to the flow direction, *Phys. Fluids*, 2007, 19, 093603.

[17] Lee, C., Kim, C., Maximizing the giant slip on superhydrophobic microstructures by nanostructuring their sidewalls, *Langmuir*, 2009, 25(21), 12812–12818.

[18] Cassie, A. B. D., Baxter, S., Wettability of porous surfaces, *Trans. Faraday Soc.*, 1944, 40, 546–551.

[19] Wenzel, R. N., Resistance of solid surfaces to wetting by water, *Ind. Eng. Chem.*, 1936, 28(8), 998–994.

[20] Poetes, R., Holtzmann, K., Franze, K., Steiner, U., Metastable underwater superhydrophobicity, *Phys. Rev. Lett.*, 2010, 105(16), 166104.

[21] Samaha, M. A., Tafreshi, H. V., Gad-el-Hak, M., Sustainability of superhydrophobicity under pressure, *Phys. Fluids*, 2012, 24(11), 112103.

[22] Samaha, M. A., Tafreshi, H. V., Gad-el-Hak, M., Inuence of flow on longevity of super-hydrophobic coatings, *Langmuir*, 2012, 28(25), 9759–9766.

[23] Bobji, M. S., Kumar, S. V., Asthana, A., Govardhan, R. N., Underwater sustainability of the "Cassie" state of wetting, *Langmuir*, 2009, 25(20), 12120–12126.

[24] Sakai, M., Yanagisawa, T., Nakajima, A., Kameshima, Y., Okada, K., Effect of surface structure on the sustainability of an air Layer on superhydrophobic coatings in a water–ethanol mixture, *Langmuir*, 2008, 25(1), 13–16.

[25] Samaha, M. A., Ochanda, F. O., Tafreshi, H. V., Tepper, G. C., Gad-el-Hak, M., *In Situ*, non-invasive characterization of superhydrophobic coatings, *Rev. Sci. Instrum.*, 2011, 82, 045109.

[26] Ng, C-O., Wang, C. Y., Stokes shear flow over a grating: Implications for superhydrophobic slip, *Phys. Fluids*, 2009, 21(1), 013602.

[27] Jeong, J-T., Slip boundary condition on an idealized porous wall, *Phys. Fluids*, 2001, 13, 1884–1890.

[28] Byun, D., Park, H. C., Drag reduction on micro-structured superhydrophobic surface, in: Proceedings of the 2006 IEEE International Conference on Robotics and Biomimetics, *IEEE.*, 2006, 818–823.

[29] Bejan, A., *Convection Heat Transfer*, 3rd edn., John Wiley & Sons, Hoboken, New Jersey, USA, 2004.

[30] Eckert, E., Gross, J. F., *Convection Heat Transfer*, McGraw-Hill Book Company, New York, New York, USA, 1963.

[31] Bergman, T. L., Lavine, A. S., Incropera, F. P., DeWitt, D. P., *Fundamentals of Heat and Mass Transfer*, 7th edn., John Wiley & Sons, Hoboken, New Jersey, USA, 2011.

[32] Martin, M., Boyd, I., Momentum and heat transfer in a laminar boundary layer with slip flow, *J. Thermophys. Heat Tr.*, 2006, 20(4), 710–719.

[33] Martin, M., Boyd, I., Falknerskan flow over a wedge with slip boundary conditions, *J. Thermophys. Heat Tr.*, 2010, 24(2), 263–270.

[34] Navier, C. L. M. H., Memoire sur les lois du mouvement des fluides, *Mem. Acad. Sci. Inst. France*, 1893, 6, 389–440.

[35] Lauga, E., Brenner, M., Stone, H. A., Microfluids: the no-slip boundary condition, in: A. Y. C. Tropea, J. Foss (Eds.), *Handbook of Experimental Fluid Dynamics*, Springer, New York, New York, USA, 2007.

[36] Lauga, E., Stone, H. A., Effective slip in pressure-driven stokes flow, *J. Fluid Mech.,* 2003, 489(8), 55-77.

[37] Schlichting, H., *Boundary-Layer Theory,* 7th edn., McGraw-Hill, New York, USA, 1979.